Detailed Investigation of the Interplay Between the Thermal Decay of the Low Temperature Metastable HS State and the Thermal Hysteresis of Spin-Crossover Solids

Nicolas Paradis, Guillaume Chastanet, Tatiana Palamarciuc, Patrick Rosa, François Varret, Kamel Boukheddaden, Jean-François Létard

Detailed investigation of the Interplay between the thermal decay of the low temperature metastable HS state and the thermal hysteresis of spin-crossover solids.

Nicolas Paradis,[a] *Guillaume Chastanet,**[a] *Tatiana Palamarciuc,*[a,†] *Patrick Rosa,*[a] *François Varret,**[b] *Kamel Boukheddaden,*[b] *and Jean-François Létard* [a]

[a] CNRS, Université de Bordeaux, ICMCB, 87 avenue du Dr. A. Schweitzer, Pessac, F-33608, France E-mail: guillaume.chastanet@icmcb.cnrs.fr

† Department of General and Analytical Chemistry, State University of Moldova, 60, street A. Mateevici, Chisinau, Moldavia

[b] Groupe d'Etude de la Matière Condensée (GEMaC), CNRS-UMR 8635 Université de Versailles Saint-Quentin, 78035 Versailles, France E-mail : francois.varret@uvsq.fr

Coordination chemistry, Spin-Crossover, Iron(II), Metal dilution, Photomagnetism, Regime change

Abstract: The magnetic and photomagnetic properties of a series of metal diluted spin-crossover complexes, $[Fe_xMn_{1-x}(dpp)_2(NCS)_2].py$ (dpp = dipyrido[3,2-a:2',3'-c]phenazine and py = pyridine), have been investigated and compared to the thermally quenched state behaviour. The aim of shifting the thermal decay temperature *T(LIESST)* into the quasi-static hysteresis range was reached for these strongly cooperative materials. A detailed investigation of the isothermal relaxations of the metastable HS state was made and compared to simulations. The theoretical investigation based on the macroscopic master equation was focused on the regime change generated by the meeting of *T(LIESST)* and the thermal hysteresis range.

Introduction

Optical addressing with molecular switchable materials is an exciting challenge for information processing. In that sense, widely investigated materials are spin-crossover (SC) solids,[1] which are able to switch their electronic configuration between high-spin (HS) and low-spin (LS) states under an external perturbation such as temperature, pressure, light or magnetic field. Optical addressing in these materials is accessible by different ways[2,3] among which the so-called LIESST (Light-Induced Excited Spin-State Trapping) and reverse-LIESST effects.[4] The former effect is based on the long lifetime of the metastable spin state at low temperature, and competes with spin state relaxation which may be thermally activated, so as to result in a temperature range above which optical addressing is no longer easily feasible. This temperature range, however, depends on the experimental kinetics, and for this reason a standard heating procedure was introduced by Létard et al. in terms of a *T(LIESST)* value,[5] associated with the thermal decay of the photo-excited metastable state.

T(LIESST) was defined as the temperature value at which occurs the inflexion point of $\gamma_{HS}(T)$ (that is the minimum of $d\gamma_{HS}(T)/dT$), where γ_{HS} is the HS fraction, for a constant temperature scan rate. Based on this approach, a large number of SCO materials have been compared and an inverse *T(LIESST)* relationship to the thermal spin-transition temperature ($T_{½}$) has been evidenced,[6,7] in qualitative agreement with the inverse energy gap law.[8] A detailed analysis of this experimental relationship allowed the identification of crucial chemical parameters for increasing the *T(LIESST)* values, from 60 K in the late 90's to 130 K for pure iron(II) SC materials,[9] and even 150 K in Prussian Blue analogues[10]. The highest value found up to now for a molecular cluster is about 180 K.[11] Clearly, the *T(LIESST)* limit seems to be not yet reached. The low-temperature metastable HS state may also be obtained by fast cooling from the high-temperature HS phase when the temperature interval between the thermal hysteresis and *T(LIESST)* is not too large. It then leads to a thermal decay temperature denoted *T(TIESST)*, for "thermally-induced excited spin state trapping". It is worth noting that such a distinction with respect to *T(LIESST)* is not relevant for the simple models used here, especially when no structural differences are observed between both states, which ensure that the metastable states reached are similar.

The aforementioned constant increase in *T(LIESST)* values led us to address the particular situation where it meets the thermal hysteresis range. For simplicity, we denote this situation the *T(LIESST)* – TH overlap. We investigated it for several years in different systems with various degrees of cooperativity. Indeed, cooperative effects within a SC material may be accounted for by elastic phenomena due to the volume difference between HS and LS molecules. The intermolecular interactions mediating cooperativity may be weak such as hydrogen bonds, π-π stacking… as well as covalent interactions in the case of extended networks. These interactions also influence the photo-induced process as well as the lifetime of the photo-induced state through self-accelerated behaviours.[8,12] We already reported

several examples of the interplay between the *T(LIESST)* and the SC curve in non-cooperative materials,[13] in systems with abrupt multi-steps character[14] or with small thermal hysteresis loops[15,16]. We now focus our attention on the overlap in systems with wide hysteresis loops. Indeed, from our previous theoretical study based on mean-field simulations[17] evidenced a peculiar feature denoted "bifurcation effect" which occurs when *T(LIESST)* meets the thermal hysteresis range, was observed for strongly cooperative systems. In fact, the *T(LIESST)* value increases upon increasing heating scan rate up to a maximum value. Figure 1 reports this observation. Moreover, this implies a discontinuity in the *T(LIESST)* vs $T_{1/2}$ plot. This bifurcation effect leads to a "regime change" which is of central interest in the present study. Indeed, the usual situation, *T(LIESST)* << $T_{1/2}$ (the thermal transition temperature), corresponds to the decay of a metastable HS state towards a stable LS state. On the contrary, in the case of *T(LIESST)* – TH overlap, the system is no longer attracted by the stable LS state, but by the HS state, which may be either metastable in the range $T_{1/2}(\downarrow)$ - $T_{1/2}$ or thermo-dynamically stable above $T_{1/2}$ (where $T_{1/2}(\downarrow)$ and $T_{1/2}(\uparrow)$ are the switching temperatures of the cooling and warming branches of the hysteresis, respectively, and $T_{1/2}$ is roughly equal to $(T_{1/2}(\downarrow) + T_{1/2}(\uparrow))/2$). The decay temperature associated with this novel regime should be better termed pseudo-*T(LIESST)*. The regime change, which is a phase transition, accordingly may be termed true to pseudo *T(LIESST)* regime change.

The interest of such overlap in highly cooperative materials lies in the observation of hidden magnetic phase in Prussian Blue analogues.[18] In fact in $Rb_xMn[Fe(CN)_6]_{(x+2)/3}.zH_2O$ materials, le rubidium ratio tuned the position and width of the thermal hysteresis allowing a complete overlap of the *T(LIESST)-TH*. It results in a paramagnetic state that can be switched into a diamagnetic state by light in a specific temperature range that correspond to the hidden

hysteresis loop. Therefore the aim of our study is to fully understand the mechanisms involved in the overlap and to prepare good candidates for a further study on hidden phases.

Therefore, we investigate the strongly cooperative spin-crossover compound, $[Fe(dpp)_2(NCS)_2].py$ (dpp = dipyrido[3,2-a:2',3'-c]phenazine and py = pyridine, Scheme 1) which exhibits a 40 K wide hysteresis loop centered at 145 K with a metastable HS state previously observed up to 100 K. [19,20] The most convenient way to tune the overlap is to use the metal dilution approach, which is known to mainly affect the transition temperature,[21] here denoted $T_{1/2}$ and the width of the thermal hysteresis loop. The insertion of guest ions with ionic radius close to or larger than HS Fe(II) tends to favor the HS phase and therefore to decrease $T_{1/2}$. Correlatively, according to Hauser's analysis of diluted systems,[22] it is expected to raise the molecular energy barrier and consequently to slow down the HS $\rightarrow$ LS relaxation, that is finally raise the *T(LIESST)* value, in agreement with the inverse gap law.[23] But the substitution of iron (II) by non- SC active ions also breaks the cooperative interactions and tends to lead to gradual spin-crossover. In any case, our previous experimental studies showed that the decrease of the cooperative interactions indeed reduced the self-acceleration effect but did not really affect the *T(LIESST)* values which remained almost constant upon metal dilution.[13] Therefore, the $[Fe(dpp)_2(NCS)_2].py$ which displays a broad thermal hysteresis at low temperature is a good candidate for tuning the *T(LIESST)* – *TH* overlap, by using small amounts of the larger Mn(II) ion as a doping guest.

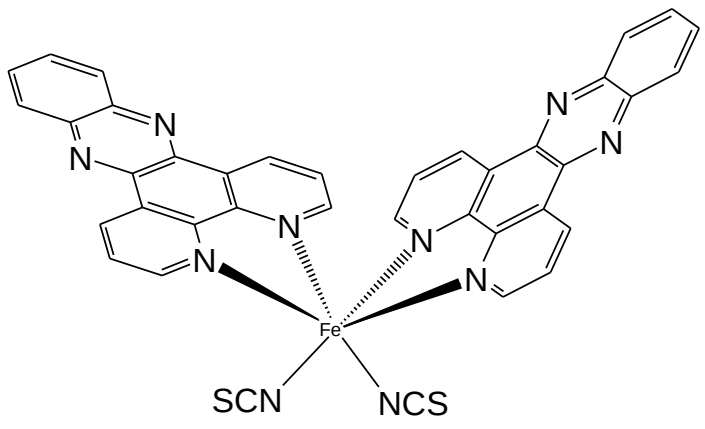

Scheme 1: Scheme of the $[Fe(dpp)_2(NCS)_2]$ unit.

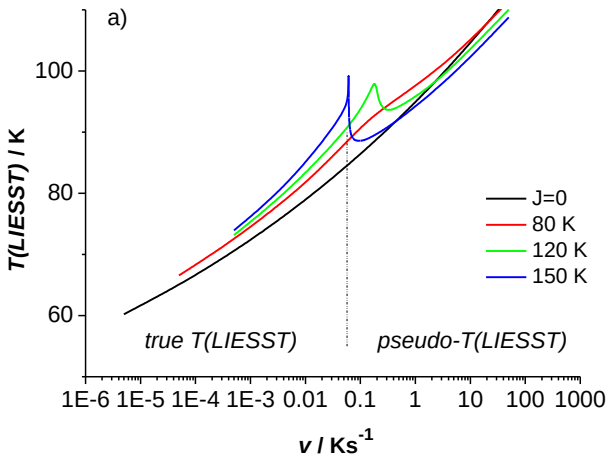

Figure 1: (a) The temperature scan-rate dependence of *T(LIESST)* plotted using the output values of ref 17; The regime change is illustrated by striking distortions of the plots for cooperative systems. Above the threshold value J ~ 1.4 $T_{1/2}$, discontinuities are observed.

Results and Discussion

The synthesis of the $[Fe_xMn_{1-x}(dpp)_2(NCS)_2]$.py family was adapted from previously described method.[19] The compositions were determined by chemical analysis (see experimental section) as x = 1 (**1**), x = 0.978 (**2**), x = 0.957 (**3**), x = 0.930 (**4**), x = 0.899 (**5**), x = 0.880 (**6**) and x = 0 (**7**). X-ray powder diffractograms were recorded on each solid solution (fig. SI-1) revealing that **1-6** are isomorphous and correspond to the structure already reported for **1**.[24-26] The powder spectra were refined using the Le Bail method on the basis of the known structure and the evolution of the cell parameters is reported in table SI1 of supplementary informations. Concerning the pure manganese compound, **7**, its diffraction

pattern slightly differs from the one of the pure iron compound indicating some structural differences.

Magnetic and photomagnetic properties.

We carried out photomagnetic measurements at the temperature scan rate of 0.4 K. min^{-1}, in successive cooling and warming modes (Figure 2).[27] As already reported[19], compound **1** exhibits a complete spin-crossover from a $\chi_M T$ value of 3.5 cm^3 K mol^{-1} at room temperature to almost zero at low temperature. The spin transition temperatures are $T_{1/2}(\downarrow)$ = 126 K and $T_{1/2}(\uparrow)$ = 163 K, defining a sharp hysteresis loop, 37 K wide. For compound **7**, the $\chi_M T$ value is equal to 4.4 cm^3 K mol^{-1}, as expected for an octahedral d^5 ion with g = 2, and remains almost constant over the whole temperature range (Figure SI-2). Regarding the $[Fe_{1-x}Mn_x]$ diluted systems, the $\chi_M T$ product increases with metal dilution due to the paramagnetic contribution of the manganese (II) ion (d^5, S = 5/2). For convenience, this Mn-contribution of the Mn(II) ions was removed according to equation 1 so as to determine the $(\chi_M T)_{Fe}$ values, which are, in first approach, proportional to the HS fraction γ_{HS}. This simple approach discards the low-temperature magnetic effects (zero-field splitting, magnetic interactions) which actually are negligible in the temperature range of interest here, T > 50 K.

$$\chi_M T = x.(\chi_M T)_{Fe} + (1-x).(\chi_M T)_{Mn} \quad (1)$$

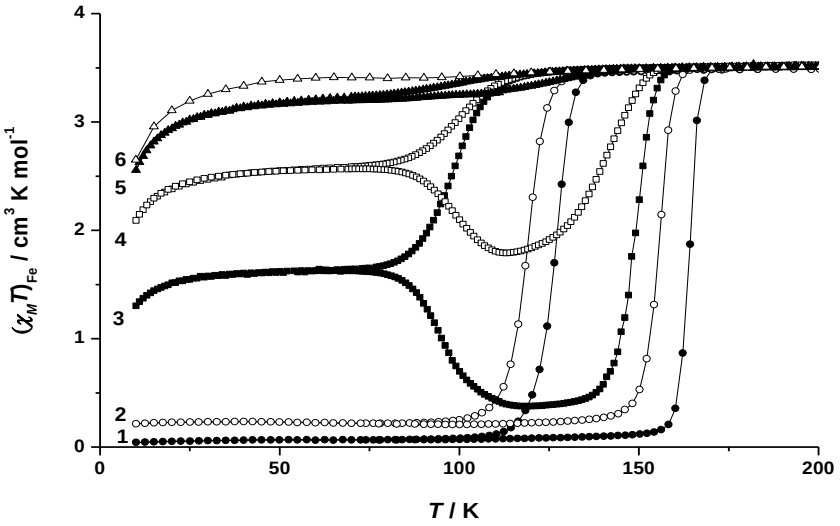

Figure 2: Thermal dependence of the $(\chi_M T)_{Fe}$ product for compounds **1**-**6**.[27a] The hysteresis loop was achieved through a succession of cooling and warming branches.

The derived temperature data are listed in table 1. At room temperature all compounds have a $(\chi_M T)_{Fe}$ value of 3.5 cm^3 K mol^{-1}, corresponding to the HS stable state of the iron (II) center (S = 2). Upon increasing metal dilution, the thermal evolution of $(\chi_M T)_{Fe}$ indicates that: (i) the spin-crossover behavior is retained up to 10 % Mn(II) and occurs with an hysteresis loop, (ii) this hysteresis is shifted toward low temperatures and progressively displays a distortion typical of kinetic effects (vide infra), (iii) a significant amount of HS residue appears at low temperature above 2.2 % Mn(II), and (iv) this residue increases so as to prevent any sizable spin-crossover in compound **6** which remains totally HS in the whole temperature range. Below 50 K, the spin states are frozen but the $(\chi_M T)_{Fe}$ contributions exhibit a typical decrease assigned to the zero-field-splitting effect of HS iron(II) ions.[28] In previous works,[13-15] we have shown that such an increase of the low-temperature residual HS fraction may originate from static and kinetic effects: the static effect follows the negative internal pressure generated by the Mn(II) ions in the Fe(II) SC matrix. Indeed the ionic radius decreases in the following order: $r(Mn^{2+})$ (r = 83 pm) > $r(Fe_{HS}^{2+})$(78 pm) > $r(Fe_{LS}^{2+})$ (61 pm).[29] The negative

internal pressure stabilizes the HS state which has a larger volume than the LS state, leading to a stable paramagnetic residue.[13,21] The kinetic effect consists in a sizable quenching of the metastable state, responsible for the typical shape of the hysteresis loops, reported for example in our previous experimental and theoretical works.[15,17]

Figure 3a for compound **3** shows hysteresis measurements performed at various rates ranging from 0.4 K.min^{-1}to 4.8 K.min^{-1}. The faster the temperature scan rate, the higher the HS residue at low temperature. At the highest rate, ~ 5 K.min^{-1}, almost no spin-crossover behaviour was observed. The minimum χ_MT values reached in the heating mode increased with the scan rate. This increase indicated the progressive impact of the overlap. Let us note that the hysteresis reported in figure 3a and 3b at 0.4 K mn^{-1} are slightly different. This illustrate the influence of the different measurement modes applied in the temperature scan rate as discussed in note 27. The settle mode was used in figure 3b instead of the sweep mode in figure 3a. This latter mode introduces some temperature drift between the measured and the real sample temperature while the scan rate is increased. This point will be detailed in the theoretical section.

We also performed isothermal relaxation experiments starting from the HS or LS states, in the range of the kinetic loops. The HS state was reached by following the cooling branch of the hysteresis, except at 100 K where a fast cooling was applied. The relaxation were followed until equilibrium was reached, and allowed to draw the quasi-static hysteresis loop, shown in Figure 3b for compound **3** and figure SI-3 for compounds **4** and **5**. Altogether, figure 3 provides striking proofs of the kinetic origin of the distortion of the experimental hysteresis loop. The data resulting from quasi-static loops have been inserted in Table 1.

Noticeably, the warming branches of the apparent and quasi-static hysteresis are almost superimposed whereas the cooling branches are well separated. This is easily explained by the thermal activation character of the relaxation rate constants. Also, consideration of the

quasi-static data leads to restore the expected decrease of the hysteresis width ΔT as a function of the Mn(II) content (see Table 1). It is also worth noting that the quasi-static conversion of compound **5** is far from complete. In other words the low-temperature HS residue contains both static and kinetic contributions.

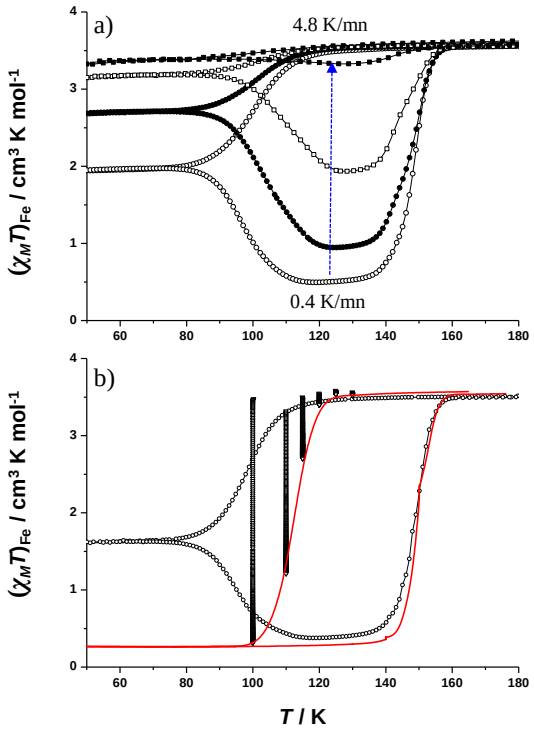

Figure 3. (a) the temperature scan rate dependence of the thermal hysteresis loop of **3** (successive cooling and warming branches, as in Figure 2); (b) selected isothermal relaxations of **3** at various temperatures below $T_{1/2}$. The red line shows the resulting quasi-static thermal hysteresis loop.

comp	**Fe (%)**	**$T_{1/2}(\uparrow)^*$ (K)**	**$T_{1/2}(\downarrow)^*$ (K)**	**$T_{1/2}{}^{a*}$ (K)**	**ΔT^{b*} (K)**	***T(LIESST)* (K)**	***T(TIESST)* (K)**
1	100	163 / 163	126 / 126	144 / 144	37 / 37	91	92
2	97.8	155 / 155	118 / 118	137 / 137	37 / 37	93	93
3	95.7	149 / 150	100 / 112	125 / 131	49 / 38	100	99

4	93	141 / 141	99 / 110	120 / 125	42 / 31	101	103
5	89.9	124 / 129	99 / 100	111 / 115	25 / 29		100
6	88						
7	0						

* values extracted from the 0.4 K mn^{-1} measurement[27a] / quasi static hysteresis curves; [a] $T_{1/2} = T_{1/2}(\uparrow) + T_{1/2}(\downarrow))/2$; [b] $\Delta T = T_{1/2}(\uparrow) - T_{1/2}(\downarrow)$.

Table 1. Summary of the experimental data.

We then investigated the behaviour of the low-temperature metastable HS state, obtained by either light irradiation or thermal trapping of the thermally-induced HS state. The basic experiments, see Figure 4, consisted in a first warming branch, the so-called "*T(LIESST)* curve", followed by successive cooling and warming branches. It is important to state that the X-ray diffraction revealed quasi-identical structures for both metastable states.[26] Accordingly their magnetic data were very similar, see Figure 2 and table 1. However the data associated with the thermal quenching process systematically met a closer agreement to the simulations. It can readily be seen that, due to bulk absorption of light, the irradiation process is hardly complete and homogeneous. In the present analysis we shall preferably use the *T(TIESST)* data, when available.

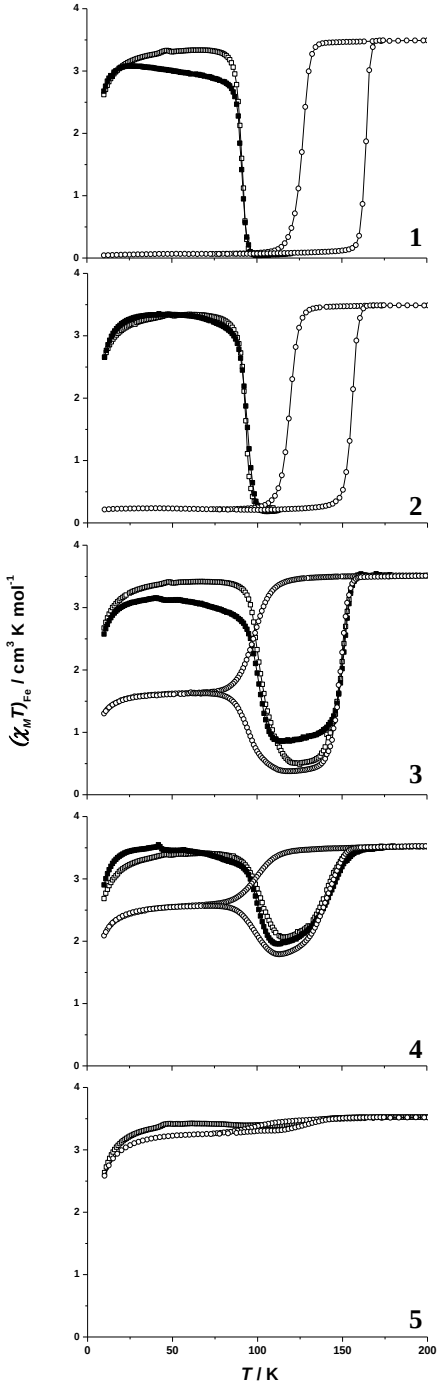

Figure 4: Thermal dependence of $(\chi_M T)_{Fe}$ for compounds **1** to **5** after fast cooling (*T(TIESST)*, □) and after irradiation (*T(LIESST)*, ■). The open circles stand for the thermal spin crossover (see fig. 1).[27a]

Upon metal dilution the *T(LIESST)* ~ *T(TIESST)* values increased from ~ 91 K in **1** to ~ 102 K in **4** (table 1). In addition to the decrease in the $T_{1/2}$ values, the increase in the

T(LIESST) values obviously favours the *T(LIESST) – TH overlap*, which mainly explains the increase of the low-temperature HS residue.

We investigated the kinetic dependence of the *T(LIESST)* ~ *T(TIESST)* values, using various temperature scan rates, see Figure 5 for **3** and figure SI-4 for **1**, **2**, **4**. Increasing the temperature scan rate increased the *T(TIESST)* value as expected[7b,c,30] and therefore the *T(TIESST)* - *TH* overlap. At the largest rate, 4.8 K.min^{-1}, the χ_MT curves of compounds **3** and **4** remained almost flat, illustrating an almost complete overlap.

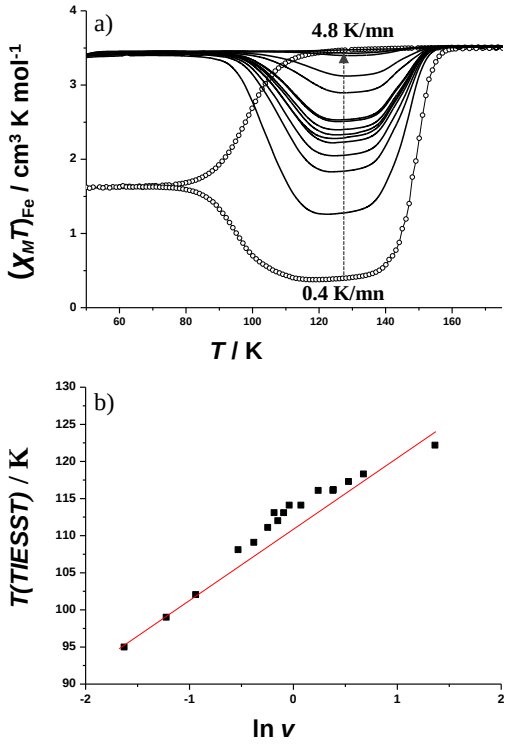

Figure 5. a) *T(TIESST)* measurements recorded at different temperature scan rates from 0.4 K/min to 4.8 K/min on **3** (full lines); the subsequent hysteresis loop is shown by open symbols; b) plot of the *T(TIESST)* value as function of the logarithm of the temperature scan rate[27b], with tentative linear regression.

The dependence of the *T(TIESST)* value as a function of the temperature scan rate *v*, see figures 5b and SI-4, shows at first sight an almost linear plot in logarithmic scale, with little

indication of the expected discontinuity reported in figure 1a. The slopes of the linear plots for compounds **1** (7.5), **2** (8.0), **3** (9.5) and **4** (6.5), do not reveal any sizable trend. In Figure 5a we show that the minimum value reached by the *T(TIESST)* curve (= first heating branch) smoothly increases with the temperature scan rate. The absence of discontinuity is assigned to a distribution of physical parameters, the presence of which is evidenced by the slope of the quasi-static hysteresis loop branches. Without distribution, te hysteresis loop would be much more abrupt. This problem will be addressed in the theoretical section.

Due to the temperature scan rate dependence of *T(TIESST), T(LIESST)* and $T_{1/2}$, some precautions are needed for establishing the "phase diagram" of the diluted system (Figure 6). This diagram is the (reverse) plot of the *T(LIESST) ~T(TIESST)* and switching temperatures ($T_{1/2}$) values as a function of the composition parameter of the series of compounds. Of course the *T(LIESST) ~T(TIESST)* data have to be selected at a unique scan rate. However the switching temperatures associated with the kinetic loops could not be followed at all scan rates because the loop vanishes at the higher rates. We therefore reported in the diagram the quasi-static data of the switching temperatures. It is shown by Figure 4 that the *T(LIESST)* data really entered the static hysteresis range under the effect of the Mn- dilution. The threshold value of Mn content which allows entering the hysteretic zone is correlated to the scan rate value: from ~ 9 % at 0.4 $K.min^{-1}$, down to ~ 3 % at 4.8 $K.min^{-1}$.

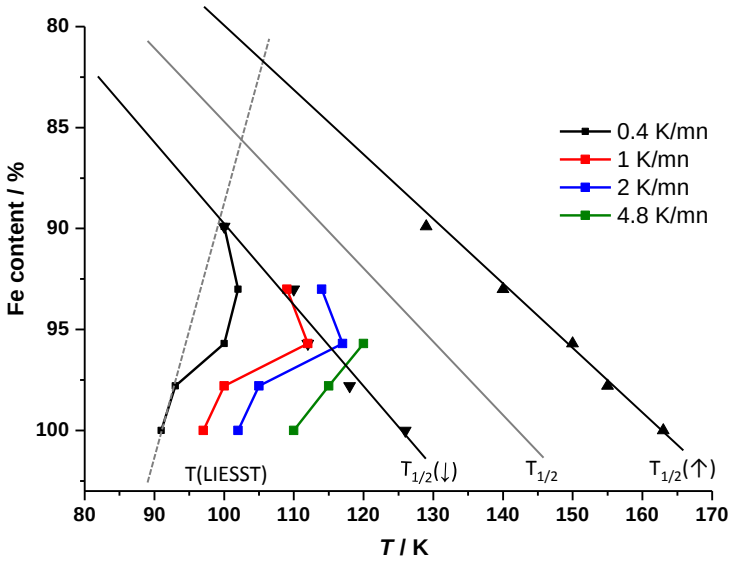

Figure 6. "Phase diagram" of $[Fe_xMn_{1-x}(dpp)_2(NCS)_2]$.py. The *T(TIESST)* values are reported for various temperature scan rates: 0.4 (black line), 1 (red line), 2 (blue line) and 4.8 (green line) K/min. The switching temperatures are shown at the quasi-static limit (data from Table 1).

Relaxation kinetics of the metastable state.

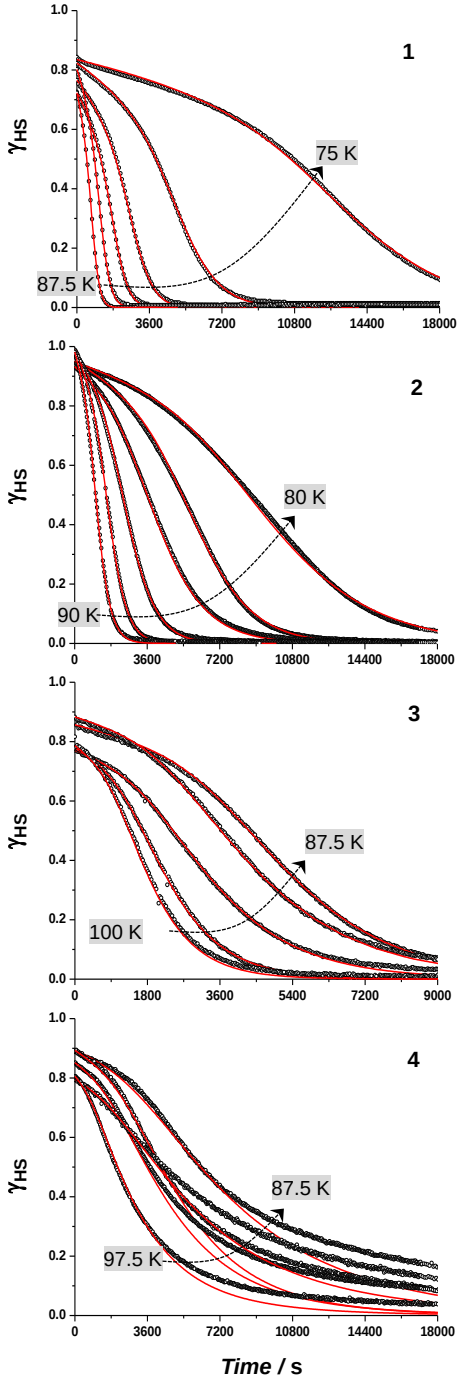

Figure 7. Time dependence at various temperatures of the switching HS molar fraction, , generated by light irradiation at 10 K for compounds **1** (every 2.5 K), **2** (every 2 K), **3** (every 2.5 K) and **4** (every 2.5 K). The symbols stand for the experimental data measured with the

SQUID magnetometer. The solid lines are the fits obtained with the model described in the text.

Figure 7 shows the relaxation kinetics of the photo-induced HS state of compounds **1-4** at several temperatures. The data resulting from a metastable HS state generated by rapid cooling (Fig SI-5) were very similar, see data on Table 2. In both cases, the kinetics of compound **5** could not be characterized due to the small amount of iron(II) metal centers involved in the SC change. The relaxation curves of compounds **1-4** strongly deviate from single exponential shape, which reveals the presence of the self-accelerated process predicted for cooperative systems.[8,12,22] This process was described as the consequence of the progressive built-up of the internal pressure in the lattice while the HS → LS spin transition proceeds, leading to a progressive decrease of the energy barrier. Accordingly, the relaxation rate $k_{HL}(T, \gamma_{HS})$ is written, in the thermal activation regime:

$$k_{HL}(T, \gamma_{HS}) = k_{HL}^{0}(T) \exp[-\alpha(T).\gamma_{HS}] \qquad (2)$$

where $\alpha(T)$ (= E_a^*/k_BT) is the "Hauser" self-acceleration factor, $k_{HL}^{0}(T)$ is the relaxation rate for a non cooperative system, and

$$\frac{d\gamma_{HS}}{dt} = -k_{HL}.\gamma_{HS} \qquad (3)$$

is the evolution equation of the system. This self-acceleration effect leads to sigmoid shaped relaxation curves.

However, this equation is valid only when the LS → HS relaxation process can be neglected. The validity condition is easily derived from the detailed balance equation $k_{HL}\ \gamma_{HS} = k_{LH}\ \gamma_{LS}$ (with the equilibrium values), leading to $\gamma_{HS}^{(equil)} \ll 1$, that is, T sizably smaller than

$T_{1/2}$. This condition is obeyed for compounds **1, 2**, but no longer for **3, 4** which display a sizeable *T(LIESST) –TH* overlap. Therefore both HS → LS and LS → HS relaxation pathways have to be taken into account, leading to the complete macroscopic master equation Eq. 4 (with the HS fraction γ_{HS} abbreviated by *n* for simplicity). This macroscopic equation is merely the kinetic extension of the usual mean-field two-level models (Ising-like, regular solutions).[31] This master equation has been recently used to simulate the *T(LIESST)* - $T_{1/2}$ overlap[17] and for calculating relaxation curves in the vicinity of the equilibrium temperature.[15b]

$$dn / dt = - n\, k_{HL} + (1 - n)\, k_{LH} \qquad (4)$$

with the relaxation rate constants

$$k_{HL}(T, n) = k_\infty exp\, (-\beta\, E_{HL}^{\,0} - \alpha\, n) = k_\infty exp\, [-\beta\, E_{HL}(n)\,],$$

$$k_{LH}(T, n) = g\, k_\infty exp\, (-\beta\, E_{LH}^{\,0} + \alpha\, n) = g\, k_\infty exp\, [-\beta\, E_{LH}\,(n)],$$

where $\beta = 1/k_B T$, $g = g_{HS}/g_{LS}$ the degeneracy ratio of the molecular spin states, k_∞ the pre-exponential factor of the relaxation rate constants characterizing the transition frequency at infinite temperature, E_{HL} and E_{LH} the molecular energy barriers with $E_{HL}\,(1/2) - E_{LH}\,(1/2) = \Delta$ the molecular energy gap = $k_B\, T_{eq}\, ln(g)$. The equilibrium temperature T_{eq} is defined by equal relaxation rates leading to equal spin population at equilibrium, $T_{eq} \sim T_{1/2}$. The cooperativity parameter $E_a^* = \alpha . k_B T$ is identified to 2*J*, the interaction parameter. Finally, $E_{HL}(0) = E_{HL}^\circ = E_a$ and $E_{LH}(0) = E_a + \Delta$. In the following presentation of results, the energies discussed are expressed in temperature unit.

However, the sigmoid shaped curves generated by Eq. 4 failed to properly simulate the experimental data of compounds **1-4,** with an increasing deviation when increasing the proportion of substituent metal. Therefore, we introduced into equation 4 a Gaussian distribution of the thermal activation energy E_a, characterized by the width parameter σ_{EB} (standard deviation). The presence of distributions gives the computed curves a stretched

character which ultimately may hide their sigmoidal nature. We used a model made of independent domains having different values of the barrier energy. The origin of this distribution may be a non-homogeneous dilution of the doping metal, as suggested in a previous work.[32] In a simple view, the sample is made of independent crystallites with slightly different contents in the doping metal. The best simulations using the present model are reported in figure 7 and SI-5; the parameters extracted from the resulting Arrhenius plots are summarized in table 2. The relevance of the model obviously seems to be limited to compounds **1-3**. The reason for the lack of success for compound **4** presumably is the large overlap with the thermal hysteresis and the local disorder in the concentrations of metal dilution. It is well known that the macroscopic (mean-field) models are not suited to describe the process of the thermal spin transition. This point will be addressed in the coming Theoretical Section.

Table 2. Kinetics parameters from simulations using Eq. 3 including energy barrier distributions for the photo-induced and thermally-quenched HS states.

	Photo-induced state				**Thermal quenched state**			
Sample	**E_a (K)**	**k_∞ (s^{-1})**	**E_a* (K)**	**σ_{EB} (K)**	**E_a (K)**	**k_∞ (s^{-1})**	**E_a* (K)**	**σ_{EB} (K)**
1	1265	160	420	26	1345	723	420	46
2	1310	215	475	39	1275	152	500	42
3	690	0.04	540	55	1075	4.07	545	66
4	455	0.001	455	79	1025	3.07	430	82

The results of the fitting procedure are discussed as follows:

(i) The data obtained for the photo-induced state (Figure 7) and for the thermally quenched state (Figure SI-5) are very similar, (table 2). However, there are sizable differences for the pre-exponential factor k_∞, which actually was obtained within a poor accuracy through a bold extrapolation of the linear fit of the Arrhenius plot (Figure SI-6).

(ii) The distribution width σ_{EB} sizably increases as a function of the doping metal content for both the photo-induced and the thermally quenched states, from 30 K for **1** up to ~ 82 K for **4**. At first order, the obtained σ-value is proportional to the content in doping metal, thus suggesting that the relative dispersion of composition remains basically the same through the series of compounds. Of course this effect of composition distribution adds up to the effect of intrinsic defects, which certainly are present in the pure compound **1**, as evidenced by the non-zero σ-value.

(iii) The cooperativity parameter E_a* increases from **1** (~ 420 K) to **3** (~ 545 K). Usually, metal dilution tends to decrease the cooperative interactions and therefore should lower the E_a* value. The opposite behaviour is observed in the present case and agrees with the previous observation reported on the $[Fe_xMn_{1-x}(bpp)_2](BF_4)_2$ family.[15b] This might suggest that, in addition to diluting the interactions, metal dilution impacts the internal pressure effect *via* a change in the elastic properties of the lattice.

(iv) The activation energy E_a decreases significantly upon metal dilution from **1** (around 1300 K) to **4 (**around 430 or 1000 K). This is in contradiction with the decrease in $T_{1/2}$ which was expected to increase E_a through the inverse energy gap law. However the fitted values of the parameter E_a are strongly correlated to those of k_∞ which actually were found with an extremely large variation, and may cast some doubt on the apparent decrease of the activation energy. In addition, the energy barrier value as well as the degeneracies g_{HS} and g_{LS} may be sensitive to variations in the elastic properties of the lattice, resulting in an increase of the cooperativity for low dilution ratio.

We also analyzed the temporal dependence of the isothermal relaxations reported in Figure 3b. Satisfactory simulations were obtained by increasing very sizably the width parameter, up to σ_{EB} ~ 145 K. This increase is correlated to the change of shape of the relaxation curves which have lost their cooperative character, as we observed in previous experimental works with[33] (ii) a slower relaxation while entering into the hysteresis loop,[31d] and (iii) the presence of short range interactions due to the nucleation-growth of domains process often encountered in systems exhibiting large hysteresis loop. The plot of the fitted relaxation rate constant, k_{HL}, as function of the inverse of the temperature, (figure SI-6), evidenced a slight decrease of k_{HL} when entering the hysteresis range of **3** and **4**. This shows a stabilization of the HS metastable state in the static hysteresis range, in agreement with previous experimental results obtained by optical spectroscopy on the $[Fe(PM\text{-}BiA)_2(NCS)_2]$ compound,[33] on the diluted $[Fe_xMn_{1-x}(3\text{-}bpp)_2](BF_4)_2$ family,[15] and also with theoretical analyses.[31a]

Theoretical Section and Simulations.

In a first step, we validated the kinetic parameters deduced from the relaxation study, by reproducing the *T(TIESST)* and *T(LIESST)* curves. The parameters values for the calculations were selected as follows: E_a and k_∞ were taken from the present investigation of the relaxation kinetics; ln g was taken equal to 7, leading to an entropy change $\Delta S = R \ln g \sim 58$ J $K^{-1}mol^{-1}$ in agreement with literature values (50 – 70 J $K^{-1}mol^{-1}$); the electronic gap in first approach was derived from equilibrium temperature value, using $\Delta = T_{eq}.\ln g \sim T_{1/2}.\ln g$ (in temperature units). The agreement was satisfactory, as it will be shown in the following figures.

For the present series of compounds, we derived from Tables 1and 2 the $J/T_{1/2}$ ratios 1.4, 1.7, 2.1, 1.7 for compounds **1** to **4**, respectively. Therefore we think the effects of the regime

change should be visible in the present figure 5b, through a sizably non-linear character of the plot. We approached a reasonable simulation of the experimental data of compound **3** (Figure 8a) by combining a distribution of barrier energies and a temporal delay (fitted to 9 s) between the temperature controller and the actual temperature of the sample. This instrumental delay adds up to the kinetic process of relaxation, it introduces in first approach a temperature correction which is proportional to the temperature scan rate.[31d] An effect of such delay could be seen in figures 3a and 3b. In figure 3a the 0.4 $K.mn^{-1}$ measurement was performed using a constant temperature scan rate (sweeping mode of the SQUID magnetometer as discuss in note 27) whereas in figure 3b a settle mode was used. This latter mode lets time to the temperature to be stable which is not the case in the sweeping mode, introducing consequently a drift in temperature. In figure 3a and 3b, depending on the temperature scan rate mode used, the 0.4 $K.mn^{-1}$ curve is clearly different especially the low temperature $\chi_M T$ value. We also followed the evolution of the n minimum value of the *T(LIESST)* curve as a function of the scan rate: in Figure 8b we reported simulations of the experimental data of compound **3**. The simulations revealed to be very sensitive to the kinetic parameters (E_a, k_∞) as well as to the width parameter σ_{EB}. Noticeably, the best-fit parameter set had to be modified with respect to that of Figure 8a. This confirms the shortcomings of the mean-field type model. In particular the larger σ_{EB} value means that further distributions should be included, as a consequence of the overlap with the thermal hysteresis. Indeed, the bent shape of the quasi-static loop implies a distribution of static parameters (T_{eq}, J). The complex problem of joint distributions was not worth addressing here due to the shortcomings of the present mean-field model (see below).

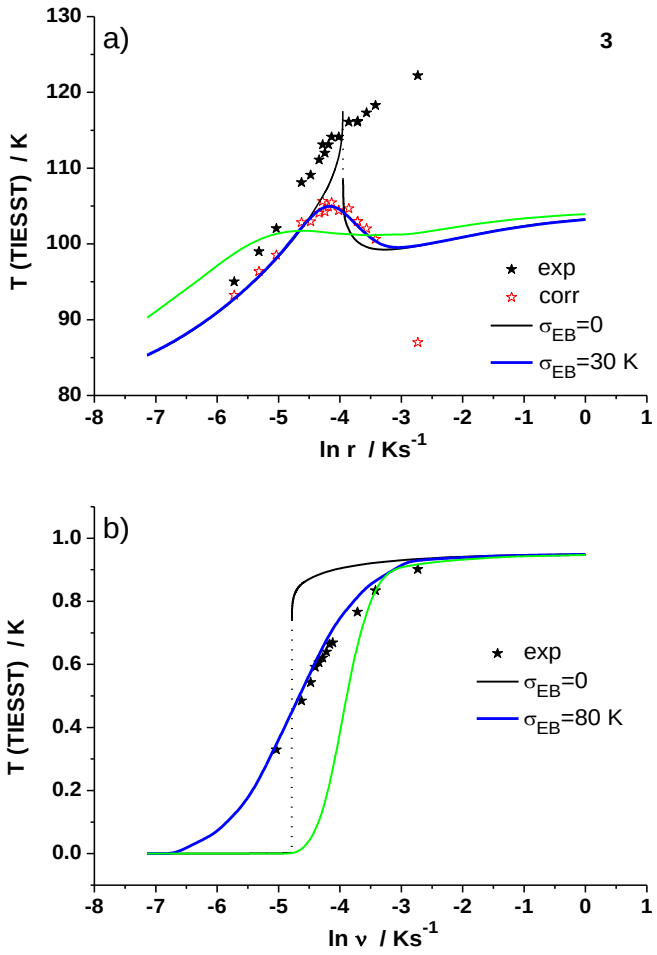

Figure 8: Experimental (★) and corrected data using the delay discussed in the text (☆) for compound **3** compared to simulations based on Eq. 3: (**a**) *T(LIESST)* values , (**b**) γ_{HS} minimum values. Blue curves are obtained with a distribution of barrier energies over independent domains. Input parameter values were T_{eq} = 135.5 K, E_a* = 2J = 547 K, k_∞ = 40 s^{-1} for both data, but the energy barrier values and distribution width parameters were separately tuned for figures a, b: E_B = 1380 K (E_a = 906 K) and 1460 K (E_a = 986 K), σ_{EB} =30 K and 80 K, respectively. The green line shows for each figure the curve computed with the parameter set tuned for the other figure.

We also examined the phase diagram of Figure 7 and noticed the non-linear character of the *T(LIESST)* plot, which suggested the occurrence of the regime change. This was

confirmed by simulations based on interpolations of all parameter values over the composition parameter. In Figure 9 we show that the theoretical discontinuity can be smeared out by the distribution effect, so as to reach a convenient agreement with the experimental data. On increasing the temperature scan rates the discontinuity is shifted closer to the T_{eq} line, but not beyond this line. However the *T(LIESST)* values can completely cross the hysteresis domain.

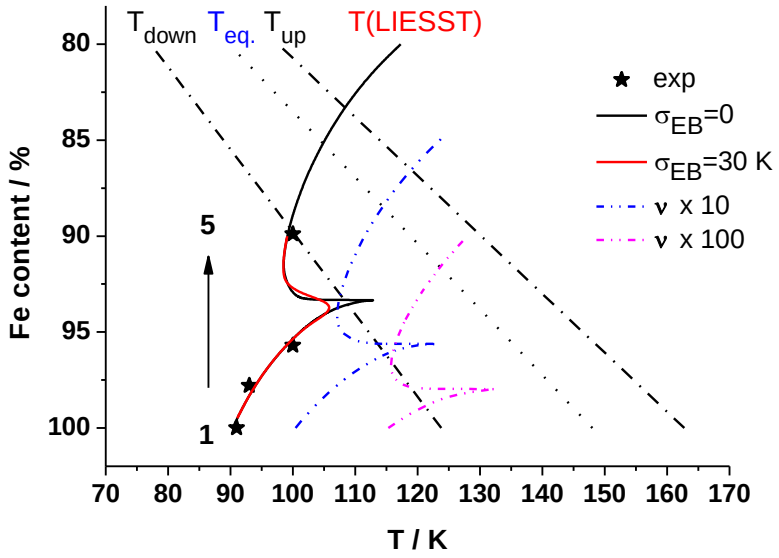

Figure 9: Phase diagram of the diluted system, computed using Eq.3 with and without distributions, compared to the experimental data of Figure 6. The theoretical curves without distribution have been computed for 3 different temperature scan rates.

We finally tried to simulate the complex curves combining the *T(LIESST)* branch and the subsequent thermal loop shown in Figure 4. Figure 10 reports the simulation with a rather good agreement with the experimental data, with however ad-hoc values of the cooperative parameters, which noticeably differ from those previously used for the *T(LIESST)* curve. This discrepancy between the cooperative parameters associated with the kinetic behavior and the ones with the static hysteresis is already known.[35] In addition, it is clear that the mean-field

model lacks the correlation effects which are the key ingredients of the nucleation and growth process associated with the first-order character of the spin transition. This nucleation and growth mechanism was evidenced by detailed investigations (X-ray diffraction,[36] optical microscopy[37]) of single crystals.

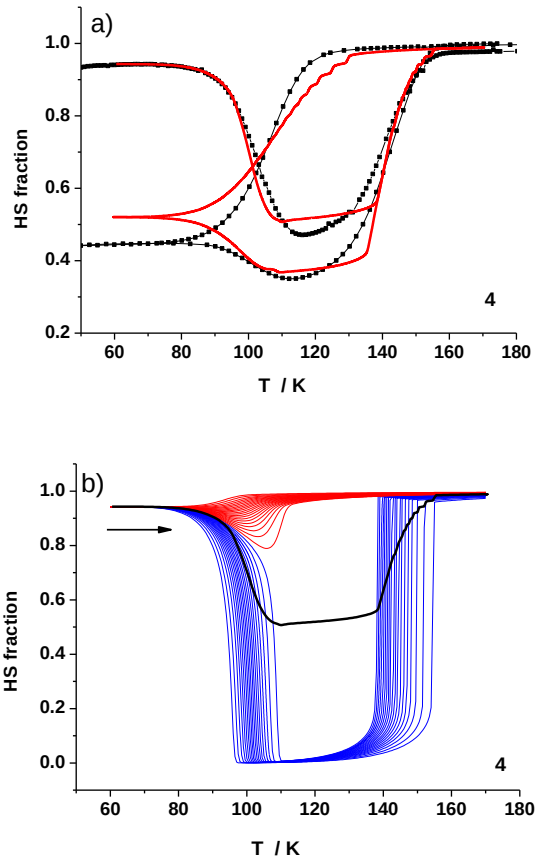

Figure 10 : Complete thermal behaviour of compound **4**, simulated with a distribution of equilibrium temperatures over independent domains, T_{eq} = 124 K, σ_{Teq} = 10 K, E_a* = 2J = 460 K, E_B = 1460 K (E_a = 1025 K), k_∞ = 30 s^{-1}, v = 0.4 K/min : **(a)** the total signal of compound **4** over 3 successive temperature scans ; (**b**) the separate signals of the independent phases with the distributed activation energy values (coloured curves) and their mean envelope (black curve) for the *T(LIESST)* branch. The bifurcation effect associated with the regime change is evidenced (different behaviour between blue and red curves). The domains following the true or pseudo *T(LIESST)* regime, leading to respectively blue and red curves, are in the ratio ~1:1.

Discussion.

We have shown that the *T(LIESST)* values can cross the thermally-induced hysteretic region. This work complete our previous investigations[15] and the observations of Hauser et coll. on $[Fe_xZn_{1-x}(bbtr)_3](Anion)_2$ systems (bbtr = 1,4-di(1,2,3-triazol-1-yl)butane and Anion is BF_4^- or ClO_4^-).[33,38,39] However this situation generates problems from both theoretical an experimental viewpoints. The theoretical point is the regime change from true to pseudo-*T(LIESST)* which occurs before the equilibrium temperature is reached. This is due to the metastable character of the HS state in the quasi-static loop, which behaves as an "attractor" for the out-of-equilibrium HS state generated at low temperature. The impact of the regime change upon the *T(LIESST)* value induces deviations from the simple linear behaviors assumed so far, for example the "dilution phase diagram" and the *T(LIESST)*/$T_{1/2}$ plot. The experimental point is that the variations of n (or γ_{HS}) become extremely small and hardly measurable.

We now discuss the different ways to generate the *T(LIESST)~T(TIESST)*- TH overlap. The first one is the chemical approach, illustrated in this work by Figure 4. Due to the importance of kinetic effects a second way consists in increasing the temperature scan rate, as shown in this work by Figure 5. A further way consists in applying a continuous light irradiation in the visible region, able to generate at low temperature the LIESST effect. This irradiation also generates the light-induced thermal hysteresis (LITH) in the case of cooperative compounds.[5,40] The thermal hysteresis loop is obviously downward shifted by light (because of both the photo-excitation and photo-heating effects) and previous theoretical work predicted a complex interplay between the LITH and TH loops.[31] In addition, the intensity of light varies through the sample due to bulk absorption of light. We recorded the LITH - TH coupled loops for compound **4** (Figure 11). The shift of the TH loop is clearly shown and

the overlap of the LITH and TH effects is evidenced by the large upraise of the γHS minimum values. We applied equation 4 completed as follows: $k_{LH}(T,n) = g\, k_\infty \exp(-\beta E_{LH} + \alpha n) + k_{opt}$, where k_{opt} is the LS → HS conversion constant rate due to irradiation, which can be determined independently by photo-excitation experiments at low temperature. We actually obtained very poor simulations, see Figure 11. We think this is due to the lack of correlations in the model but also to the fact that the bleaching effect was not accounted for. Indeed large correlations are expected during the long-lasting relaxation under light. However, the simple simulations performed here unambiguously show that the fraction of domains in the pseudo *T(LIESST)* regime is larger than that of Figure 10. This means that irradiation increases the *T(LIESST)* – TH overlap.

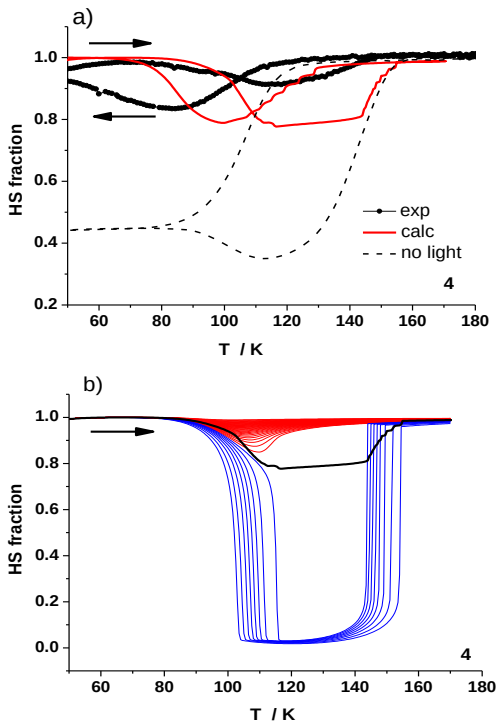

Figure 11 : **(a)** The *LITH* and *TH* loops (black symbols) of compound **4** under light, compared to the thermal spin transition (slashed line). The red line results from simulation with the set of parameters used for Figure 10, completed by the photo-excitation rate constant k_{opt} = 0.001 s^{-1} consistent with the experimental kinetics of the *LIESST* effect; (**b**) The

separate signals of the independent phases with the distributed activation energy values (colour curves) and their mean envelop (black curve) for the *T(LIESST)* branch. The ratio of domains following the pseudo *T(LIESST)* regime, (red curves) has increased up to ~ 4:1 under the effect of light.

Regarding our seeking for hidden phase, compound **6** looks like a good candidate for such observation. The best conditions for that have to be found in the expected 95-110 K region.

Conclusion

We have investigated a new series of diluted compounds in order to follow the behavior of the metastable HS state when the decay temperature *T(LIESST)*, *T(TIESST)* is raised at the vicinity of the thermal spin transition. We have evidenced specific kinetic effects associated with the overlap of the *T(LIESST)*, *T(TIESST)* and thermal hysteresis, which originate from a progressive stabilization of the metastable HS state. The present investigation has documented the regime change from the usual to the pseudo-*T(LIESST)*. Comparison between experiment and simulation using a kinetic extension of the usual 2-level macroscopic model has shown that the mean field approach is not ideally suited to describe the overlap effects. However, it qualitatively reproduced the most important features of the phenomenon, for example the dependence of the data upon the temperature scan rate, with the typical deviations associated with the regime change. More realistic models for the overlap effects should include correlations and should take into account of the structural response to the kinetic effects, leading presumably to a two order parameters problem. This obviously is a big challenge, presumably easier to address by using single crystals which should minimize distributions of structural origin.

Experimental Section

Synthesis of the dpp ligand (dpp = dipyrido[3,2-a:2',3'-c]phenazine):

The previously described hydrothermal method was followed to synthesize ligand dpp.[40] A mixture of 1,10 phenanthroline-5,6-dione (580 mg, 2.75 mmol) and 1,2-phenylenediamine (320 mg, 3 mmol) in a mixed solution of 60 mL H2O and 7 mL ethanol was heated at 180 °C for one night in a stainless steel pressure reactor. Pressure during the reaction rises to between 11 and 12 bars. The yellow-white powder obtained after cooling at room temperature was filtered, washed with cold ethanol and diethyl ether, then recrystallized in methanol. Yield: 75 %. Elemental Analysis Calc. for $C_{18}H_{10}N_4.H_2O$ (300.31 $g.mol^{-1}$): C, 71.99; H, 4.03; N, 18.66; Found: C, 71.54; H, 3.95; N, 18.72.

Synthesis of complexes $[Fe_xMn_{1-x}(dpp)_2(NCS)_2].py$

The synthesis of complexes is adapted from reference[17]. On one hand a solution of $[Fe_xMn_{1-x}(py)_4(NCS)_2]$ (3.5 mmol) (with py = pyridine) is prepared with the desired Fe/Mn ratio, from the reaction of $FeSO_4.7H_2O$, $MnCl_2$ with 2 equivalents of KNCS in 5 mL of methanol. The white precipitate (KCl and K_2SO_4) is filtrated off and 1 mL of pyridine is added. Yellow $[Fe_xMn_{1-x}(py)_4(NCS)_2]$ precipitates. After solvent removal under vacuum, 5 mL of pyridine are added and the mixture is heated at 85 °C until the yellow powder is solubilized. On the other hand, 2 equivalents of dpp ligand (7 mmol) are dissolved in 6 mL of hot pyridine (85°C). After half an hour, the ligand solution is added dropwise in the $[Fe_xMn_{1-x}(py)_4(NCS)_2]$ solution. A violet precipitate appears. After cooling the solution back to room temperature, the solid compound was filtered and washed with 2 mL of cold pyridine. Yield: 75-80 %. The experimental Fe/Mn ratio was determined by microprobe electron beam, and was shown to be within 5% of the salts starting ratio. Scans over 3000 μm^2 evidenced homogeneous samples, no segregation of either metal and coprecipitation of KCl. Unsuccessful mineralization prevented ICP-OES analysis, of Fe, Mn and K cations.

Homogeneity of the materials was also evidenced by CHNS elemental analysis. 7 different materials were obtained with the following composition. Elemental Anal Calc. for compound **1** $[Fe(dpp)_2(NCS)_2].py$ (815.71 $g.mol^{-1}$): C, 63.31; H, 3.09; N, 18.89; S, 7.86;; Found: C, 63.12; H, 3.11; N, 18.77; S, 8.27;; Calc. for Compound **2** $[Fe_{0.978}Mn_{0.022}(dpp)_2(NCS)_2].py.(KCl)_{0.04}$ (818.67 $g.mol^{-1}$): C, 63.09; H, 3.08; N, 18.82; S, 7.83;; Found: C, 62.82; H, 3.11; N, 18.65; S, 8.27;; Calc. for Compound **3** $[Fe_{0.957}Mn_{0.043}(dpp)_2(NCS)_2].py.(KCl)_{0.8}$ (821.63 $g.mol^{-1}$): C, 62.86; H, 3.07; N, 18.75; S, 7.81;; Found: ; C, 62.78; H, 3.13; N, 18.58; S, 8.31;; Calc. for Compound **4** $[Fe_{0.93}Mn_{0.07}(dpp)_2(NCS)_2].py.(KCl)_{0.14}$ (826.08 $g.mol^{-1}$): C, 62.52; H, 3.05; N, 18.65; S, 7.76;; Found: C, 62.24; H, 2.99; N, 18.72; S, 7.81;; Calc. for Compound **5** $[Fe_{0.899}Mn_{0.101}(dpp)_2(NCS)_2].py.(KCl)_{0.2}$ (830.53 $g.mol^{-1}$): C, 62.17; H, 3.03; N, 18.55; S, 7.72;; Found: C, 62.02; H, 2.93; N, 19.24; S, 4.03;; Calc. for Compound **6** $[Fe_{0.88}Mn_{0.12}(dpp)_2(NCS)_2].py.(KCl)_{0.24}$ (833.49 $g.mol^{-1}$): C, 61.96; H, 3.02; N, 18.49; S, 7.69;; found: C, 61.55; H, 3.03; N, 18.27; S, 7.96;; Calc. for Compound **7** $[Mn(dpp)_2(NCS)_2].py.(KCl)_{1.2}$ (904.26 $g.mol^{-1}$): C, 57.11; H, 2.79; N, 17.04; S, 7.09;; Found: C, 57.14; H, 2.83; N, 16.93; S, 7.55.

Physical measurements.

CHNS elemental analyses were performed on a ThermoFisher FlashEA-1112 microanalyzer with a Mettler Toledo MX5 microbalance. Powder X-ray diffraction data were recorded using a PANalytical X'Pert MPD diffractometer with Bragg–Brentano geometry, Cu Ka radiation and a backscattering graphite 370 monochromator. Magnetic susceptibilities were measured in the 5-300 K temperature range, under an applied magnetic field of 1T, using a MPMS5 SQUID magnetometer (Quantum Device). The samples were precisely weighted and corrections were applied to account for the compound and sample holder diamagnetic contributions. Photomagnetic measurements were performed using a Spectrum

Physics Series 2025 Kr+ laser (λ = 676 nm) coupled via an optical fibre to the cavity of the SQUID magnetometer. The optical power at the sample surface was adjusted to 5 mW cm^{-2}, and it was verified that this resulted in a negligible change in the magnetic response due to heating of the sample. Photomagnetic samples consisted of a thin layer of compound whose weight was obtained by comparison of the thermal spin crossover curve to that of a more accurately weighed sample of the same material. Our previously published standardized method for obtaining LIESST data[3,4] was followed. After slow cooling down to 10 K, the sample, then in the low-spin state, was irradiated and the change in magnetism was monitored. Once the saturation point was reached, the laser was switched off, and temperature was raised at the standard rate of 0.3 K min–1. During the heating ramp, magnetization was measured every 1 K. *T(LIESST)* was determined from the minimum of the $\partial\chi_M T/\partial T$ vs. T plot, as previously published.[3-5] In other experiments the sample was rapidly quenched at 10 K by inserting the sample holder (in less than 10 s) from room temperature down to the SQUID cavity previously cooled at 10 K. The same procedure than for *T(LIESST)* was then followed.

Acknowledgements

The authors would like to thank the GDR MCM2 for giving nice opportunities to present and discuss the results, the GIS-Advanced Materials in Aquitaine (AMA), the Aquitaine Region for supporting the development of the ICPA (International Center of Photomagnetism in Aquitaine) platform at the ICMCB, the X-Ray diffraction and the chemical analyses services of the ICMCB and CECAMA. They also acknowledge the financial support of ANR-BISTAMAT (n° ANR-12-BS07-0030) and ANR-MOSE (n° BLANC7-1-187211).

Supporting Information. Supplementary informations are available free of charge via the Internet at http://pubs.acs.org."

REFERENCES

1 For general reviews on "Spin crossover in transition Metal Compounds" Gütlich, P.; Goodwin, H. A.; (Eds), Top. Curr. Chem. (2004), Springer-Verlag Berlin Heildeberg, *233-235*.

2 Boillot, M.-L.; Zarembowitch, J.; Sour, A.; in "Spin crossover in transition Metal Compounds" Gütlich, P.; Goodwin H. A. (Eds), Top. Curr. Chem. (2004), Springer-Verlag Berlin Heildeberg, *234*, 261.

3 a) Freysz, E.; Montant, S.; Létard, S.; Létard, J.-F. ; *Chem. Phys. Lett.,* **2004**, *394*, 318; b) Shimamoto, N.; Okhashi, S.-S.; Sato, O.; Hashimoto, K.; *Chem. Lett*., **2002**, 486; c) Bonhommeau, S.; Molnar, G.; Galet, A.; Zwick, A.; Real, J.A.; McGarvey, J. J.; Bousseksou, A. *Angew. Chem. Int. Ed. Engl*., **2005**, *44*, 2.

4 a) Descurtin, S.; Gütlich, P.; Köhler, C.P.; Spiering, H.; Hauser, A.; *Chem Phys Lett.* **1984**, 105, 1; b) Hauser, A.; *Chem. Phys. Lett.* **1986**, 124, 543.

5 Létard, J.-F.; Guionneau, P.; Rabardel, L.; Howard, J.A.K.; Goeta, A.E.; Chasseau, D.; Kahn, O.; *Inorg. Chem*. **1998**, 37, 4432

6 a) Létard, J.-F.; Capes, L.; Chastanet, G.; Moliner, N.; Létard, S.; Real, J.A.; Kahn, O.; *Chem. Phys. Lett*. **1999**, 313, 115; b) Marcén, S.; Lecren, L.; Capes, L.; Goodwin, H.A.; Létard, J.-F.; *Chem. Phys. Lett*. **2002**, 358, 87; (c) Shimamoto, N.; Ohkoshi, S.-S.; Sato, O.; Hashimoto, K.; *Inorg. Chem*. **2002**, *45*, 678.

7 a) Létard, J.-F.; Guionneau, P.; Nguyen, O.; Costa, J.S.; Marcén, S.; Chastanet, G.; Marchivie, M.; Capes, L.; *Chem. Eur. J.* **2005**, 11, 4582; b) Létard, J.-F.; *J. Mater. Chem*. **2006**, 16, 2550; c) Létard, J.-F.; Chastanet, G.; Guionneau, P.; Desplanches C.; "Optimising the stability of trapped metastable spin states", Ed. Halcrow, M.A. "Spin-crossover materials - properties and applications", John Wiley & Sons, Chichester, UK, **2012**,475.

8 Hauser, A.; *Coord. Chem. Rev*. **1991**, 111, 275.

9 a) Hayami, S.; Gu, Z.-Z.; Einaga, Y.; Kobayashi, Y.; Ishikawa, Y.; Yamada, Y.; Fujishima, A.; Sato, O.; *Inorg. Chem*. **2001**, *40***,** 3240; (b) Costa, J.S.; Guionneau, P.; Létard, J.-F.; *J. Phys.: Conference Series*, **2005**, *21,* 67

10 a) Shimamoto, N.; Ohkoshi, S.-S.; Sato O.; Hashimoto, K.; *Inorg. Chem.* **2002**, *41*, 678; b) Lebris, R.; Mathonière, C.; Létard, J.-F.; *Chem. Phys. Lett.* **2006**, *426*, 380

11 Li, D.; Clérac, R.; Roubeau, O.; Harte, E.; Mathonière, C.; LeBris, R.; Holmes, S. M.; *J. Am. Chem. Soc.*, **2008,** *130*, 252

12 a) Hauser, A.; *Comments Inorg. Chem.* **1995**, *17*, 17. b) Hauser, A.; Enaschescu, C.; Daku, M.L.; Vargas, A.; Amstutz, N. *Coord. Chem. Rev.*, **2006**, *250*, 1642

13 a) Baldé, C.; Desplanches, C.; Gütlich, P.; Freysz, E.; Létard, J.-F. *Inorg. Chim. Acta.*, **2008**, *361*, 3529; b) Dupouy, G.; Marchivie, M.; Triki, S.; Sala-Pala, J.; Gómez-García, C.J.; Pillet, S.; Lecomte, C.; Létard, J.-F. *Chem. Comm.* **2009**, 3404-3406; c) Baldé, C.; Desplanches, C.; Grunert, M.; Wei, Y.; Gütlich, P.; Létard, J.-F. *Eur. J. Inorg. Chem*., **2008**, 5382.

14 Money, V.A.; Carbonera, C.; Halcrow, M.A.; Howard, J.A.K.; Létard, J.-F. *Chem. Eur. J.*, **2007**, *13*, 5503;

15 a) Paradis, N.; Chastanet, G.; Létard, J.-F.; *Eur. J. Inorg .Chem*. **2012**, 3618 ; b) Paradis, N.; Chastanet, G.; Varret, F.; Létard, J.-F. *Eur. J. Inorg. Chem*. **2013**, 698.

16 Létard, J.-F.; Asthana, S.; Shepherd, H.J.; Guionneau, P.; Goeta, A.E.; Suemura, N.; Ishikawa, R.; Kaizaki, S. *Chem. Eur. J.,* **2012**, *18*, 5924;

17 Varret, F.; Boukheddaden, K.; Chastanet, G.; Paradis, N.; Létard, J.-F. *Eur. J. Inorg. Chem*, **2013**, 763.

18 a) Shimamoto, N.; Ohkoshi, S.-I.; Sato, O.; Hashimoto, K. *Inorg. Chem*. **2002**, *45*, 678; b) Ohkoshi, S.; Tokoro, H.; Utsunomiya, M.; Mizuno, M.; Abe, M.; Hashimoto, K .*J. Phys. Chem. B* **2002**, *106*, 2423; c) Tokoro, H.; Ohkoshi, S.; Matsuda, T.; Hashimoto, K. *Inorg. Chem.* **2004**, *43*, 5231; d) Tokoro, H.; Hashimoto, K.; Ohkoshi, S. *J. Mag. Mag. Mat.* **2007**, *310*, 1422; e) Tokoro, H.; Matsuda, T.; Nuida, T.; Moritomo, Y. ; Ohoyama, K. ; Loutete Dangui E. D. ; Boukheddaden, K. ; Ohkoshi, S.-I. *Chem. Mater.* **2008**, *20*, 423; f) Tokoro, H.; Ohkoshi, S. *Appl. Phys. Lett.* **2008**, *93*, 021906; g) Létard, J.-F.; Chastanet, G.; Tokoro, H.; Ohkoshi, S.-I., *submitted*.

19 Zhong, Z. J.; Tao, J.-Q.; Yu, Z.; Dun, C.-Y.; Liu, Y.-J.; You, X.-Z.; *J. Chem. Soc., Dalton. Trans.*, **1998**, 327

20 Yu, Z.; Liu, K.; Tao, J. Q.; Zhong, Z. J.; You, X. Z. *Applied Physics Letters*, **1999**, *74*, 4029

21 Ganguli, P.; Gütlich O.; Müller, E.W. *Inorg. Chem*. **1982**, *21*, 3429

22 Hauser, A.; Gütlich, P.; Spiering, H.; *Inorg. Chem*. **1986**, *25*, 4245

23 a) Englman, R.; Jortner. J.; *Mol. Phys.* **1970**, *18*, 145; b) Freed, K.F.; Jortner. J.; *J. Chem. Phys.* **1970**, *52*, 6272.

24 Kusz, J.; Zubko, M.; Fitch, A.; Gütlich, P.; *Z. Kristallogr*. **2011**, *226*, 576.

25 Shepherd, H.J.; Palamarciuc, T.; Rosa, P.; Guionneau, P.; Molnar, G.; Létard, J.-F.; Bousseksou, A. *Angew. Chem. Int. Ed. Engl*. **2012**, *51*, 3910

26 Palamarciuc*,* T.; *PhD Tesis*, University of Bordeaux, **2012**

27 a) The *T(LIESST)*, *T(TIESST)* and hysteresis measurements have been performed in settle mode of the SQUID magnetometer. The mean value 0.4 $K.min^{-1}$ for the temperature scan rate results from the average time between successive measurements. b) The specific investigations of the role of the temperature scan rate were made in sweep mode, that is, temperature is not stabilized before each measurement.

28 Kahn, O.; *Molecular Magnetism*, VCH, Weinheim New York **1993.**

29 Shannon, R. D.; *Acta Crystallographica, A* **1976**, *32*, 751.

30 Chastanet, G.; PhD Tesis, University of Bordeaux, **2002**.

31 a) I. Shteto, K. Boukheddaden, F. Varret, Phys. Rev. E 60 (1999). 5139 ; b) Boukheddaden, K.; Shteto, I.; Hôo, B.; Varret, F.; *Phys. Rev. B.* **2000**, *62*, 14796, and 14806 ; c) Varret, F.; Boukheddaden, K.; Codjovi, E.; Maurin, I.; Tokoro, H.; Ohkoshi, S.; Hashimoto, K. *Polyhedron* **2005**, *24*, 2857; d) Castro, M.; Rodriguez, J.A.; Boukheddaden, K.; Varret, F.; Tokoro, H.; Ohkoshi, S. *Eur. Phys. Lett.* **2007**, 79, 27007.

32 a) Tanasa, R.; Enachescu, C.; Stancu, A.; Linares, J.; Codjovi, E.; Varret, F. *Phys Rev. B,* **2005,** 71, 14431 ; b) Mishra, H.; Mishra, V.; Varret, F.; Mukherjee, R.; Baldé, C.; Desplanches, C.; Létard, J.-F. *Polyhedron* **2009**, 28, 1678.

33 a) Degert, J.; Lascoux, N.; Montant, S.; Létard, S.; Freysz, E.; Chastanet, G.; Létard, J.-F. *Chem. Phys. Lett.,* **2005**, *415,* 206; b) Buron-Le Cointe, M.; Hébert, J.; Moisan, N.;

Toupet, L.; Guionneau, P.; Létard, J.-F.; Freysz, E.; Cailleau, H.; Collet E. *Phys. Rev. B*, **2012**, *85*, 064114-1/9;

34 a) Chakraborty, P.; Enachescu, C.; Hauser, A.; *Eur. J. Inorg. Chem.* **2013**, 770 ; b) Chakraborty, P.; Enachescu, C.; Walder, C.; Bronisz, R.; Hauser, A.; *Inorg. Chem*. **2012**, *51*, 9714

35 a) Gawali-Salunke, S.; Varret, F.; Maurin, I.; Malarova, M.; Enachescu, C.; Boukheddaden, K.; Codjovi, E.; Tokoro, H.; Ohkoshi, S.; Hashimoto. K. *J. Phys. Chem. B.* **2005,** 109, 8251; (b) Mishra, V.; Mukherjee, R.; Linares, J.; Balde, C.; Desplanches, C.; Létard, J.F.; Collet, E.; Toupet, L.; Castro, M.; Varret , F. *Inorg. Chem*. **2008**, 47, 7577; (c) Mishra, H.; Mishra, V.; Varret, F.; Mukherjee, R.; Baldé, C.; Desplanches, C.; Létard, J.-F. *Polyhedron* **2009**, 28, 1678.

36 Pillet, S.; Hubsch J.; Lecomte, C. *Eur. Phys. J. B*, **2004**, *38*, 541.

37 Slimani, A.; Varret, F.; Boukheddaden, K.; Garrot, D.; Oubouchou, H.; Kaizaki, S. *Phys. Rev. Lett.* **2013**, *110*, 087208.

38 Chakraborty, P.; Bronisz, R.; Besnard, C.; Guénée, L.; Pattison, P.; Hauser, A.; *J. Am. Chem. Soc.* **2012**, *134*, 4049.

39 a) Chakraborty, P.; Enachescu, C.; Humair, A.; Egger, L.; Delgado, T.; Tissot, A.; Guénée, L.; Besnard, C.; Bronisz, R.; Hauser, A.; *Dalton Trans*. **2014**, *43*, 17786 ; b) Chakraborty, P.; Pillet, S.; Bendeif, E.-E.; Enachescu, C.; Bronisz, R.; Hauser, A.; *Chem. Eur. J.*, **2013**, *19*, 11418.

40 a) Desaix, A.; Roubeau, O.; Jeftic, J.; Haasnoot, J. G.; Boukheddaden, K.; Codjovi, E.; Linarès, J.; Nogues M.; Varret, F. *Eur. Phys. J. B*, **1998**, *6*, 183; b) Létard, J.-F.; Chastanet, G.; Nguyen, O.; Marcèn, S.; Marchivie, M.; Guionneau, P.; Chasseau D.; Gütlich,

P.*Monatsh. Chem.*, **2003**, *134*, 165 ; c) Enachescu, C.; Tanasa, R.; Stancu, A.; Chastanet, G.; Létard, J.-F.; Linarès J.; Varret, F. *J. Appl. Phys.*, **2006**, *99*, 08J504.

41 Che, G.; Li, W.; Kong, Z.; Su, Z.; Chu, B.; Li, B.; Zhang, Z.; Hu, Z.; Chi, H. *Synth. Commun.*, **2006**, *36*, 2519.

TABLE OF CONTENTS

We investigated the photomagnetic properties of metal diluted spin-crossover complexes $[Fe_xMn_{1-x}(dpp)_2(NCS)_2]py$, in order to document the effects of the overlap between the metastable high spin state generated by light irradiation (or by thermal trapping) and the thermal hysteresis range. Several ways for driving the metastable high-spin state into the hysteresis loop were followed and the data analyzed through theoretical studies.